Effect of Buoyancy on Three-Dimensional Flow Around a Heated Square Cylinder in Mixed Convection

Mohd Perwez Ali, Nadeem Hasan, and Sanjeev Sanghi

Abstract Three-dimensional flow around a heated square cylinder is studied using direct numerical simulation (DNS) in a mixed convective flow regime. In this study, an infinite square cylinder is immersed in horizontal free-stream crossflow (air, Prandtl number $Pr = 0.7$) at right angles to gravity. Numerical results are shown with different heat levels defined by the over-heat ratio $\epsilon = (T_w - T_\infty)/T_\infty$, where T_w and T_∞ are equal to the surface and surrounding temperature. At large-scale heating $\epsilon \sim O(1)$, the thermal straining and transport properties of the fluid particles are varied. To capture this variation, an in-house solver of the compressible flow model is employed. The compressible flow governing equations in Cartesian coordinates are transformed into a body-fitted coordinate system and solved using the flux-based particle velocity upwind-modified+ (PVU-M+) scheme. The low Mach number $M = 0.1$ is used for all computations. The results obtained using the in-house solver are validated with the values reported in the literature achieved by experimental, DNS, and Floquet methods. The disordered vortical structure of the mode B transition changes its shape and spanwise wavelength with the increase of the heating level from $\epsilon = 0$ to $\epsilon = 1$ at the Reynolds number $Re = 500$. In addition, a very significant change in the force coefficient and the vortex shedding frequency is observed upon increasing the heating level. Variations in the frequency spectra of the lift coefficient are observed with varying heating.

M. P. Ali (✉) · S. Sanghi
Indian Institute of Technology Delhi, New Delhi 110 016, India
e-mail: perwezali7@gmail.com

S. Sanghi
e-mail: sanghi@am.iitd.ac.in

N. Hasan
Aligarh Muslim University, Aligarh 202 002, Uttar Pradesh, India
e-mail: nadhasan@gmail.com

© The Author(s), under exclusive license to Springer Nature Singapore Pte Ltd. 2024

M. A. Siddiqui et al. (eds.), *Advances in Heat Transfer and Fluid Dynamics*, Lecture Notes in Mechanical Engineering, https://doi.org/10.1007/978-981-99-7213-5_11

1 Introduction

The dynamics of the three-dimensional vortex structure behind a bluff-body wake is a very interesting phenomenon. Many experimental and numerical studies have been conducted to understand the two-dimensional and three-dimensional wake dynamics behind a bluff body. Three-dimensional flow studies mostly focus on the isothermal wake behind unheated bluff bodies, especially circular and square cylinders. Only a few three-dimensional studies have been conducted around a heated cylinder in the mixed convective flow regime. However, in mixed convection, the three-dimensional flow around a heated bluff body is of great importance in engineering and industries based on applications such as electronics cooling, chemical reactors, and compact heat exchangers.

The sequence of three-dimensional transition modes with an increase in Reynolds number Re has been studied in the literature using various methods. These three-dimensional transition modes are recognized by the shape and spanwise wavelength λ_z of the vortical structure. The first transition, i.e., mode A, with longer wavelengths,$\lambda_z = 5D - 5.8D$ (where D is the side length of the square cylinder), is observed in the Reynolds number range between 150 and 200 [1–5]. For $Re = 190 - 250$, the second transition, represented by mode B, appears with a shorter wavelength $\lambda_z = 1D - 1.2D$ [1, 2, 5]. The third transition known as mode C with intermediate wavelength $\lambda_z = 2.6D - 2.8D$ between is detected using Floquet stability analysis for $Re = 200 - 215$ [2, 6]. At higher Reynolds numbers ($Re \geqslant 250$), an irregular three-dimensional instability is observed in the cylinder wake [7].

In mixed convective flow regimes, experimental and numerical studies have been performed on three-dimensional flow transitions behind a heated circular cylinder [8, 9]. In these studies, water flows perpendicular to gravity within the range of Reynolds number $75 < Re < 117$ and Richardson number range $0.35 < Ri < 2.5$. Based on these studies, it can be concluded that the three-dimensional transition with $\lambda_z = 2D$ in the heated cylinder wake, denoted as mode E, occurs at a lower Reynolds number than the mode A transition of the unheated cylinder. Arif and Hasan [10] studied buoyancy effects on the three-dimensional transition around a square cylinder, which is subjected to horizontal crossflow using air and water as working fluids. In this investigation, buoyancy effects on flow properties such as force coefficient, Strouhal number, and Nusselt number are investigated for $Re = 50 - 250$ and $Ri = 0 - 2$. In literature, three-dimensional transitions around a heated cylinder have only been studied using the Boussinesq approximation (small-scale heating scenario). In large-scale heating in mixed convection, only two-dimensional wake transitions behind a heated square cylinder have been demonstrated at $Re = 100$ using the non-Oberbeck Boussinesq model [11–13]. These studies describe the effects of buoyancy on vortex shedding and flow parameters.

In the present investigation, an infinite square cylinder is immersed in a uniform free-stream crossflow (with fluid velocity U_∞ and temperature T_∞) perpendicular to gravity (see Fig. 1a). Since the spanwise length is infinite, the three-dimensional

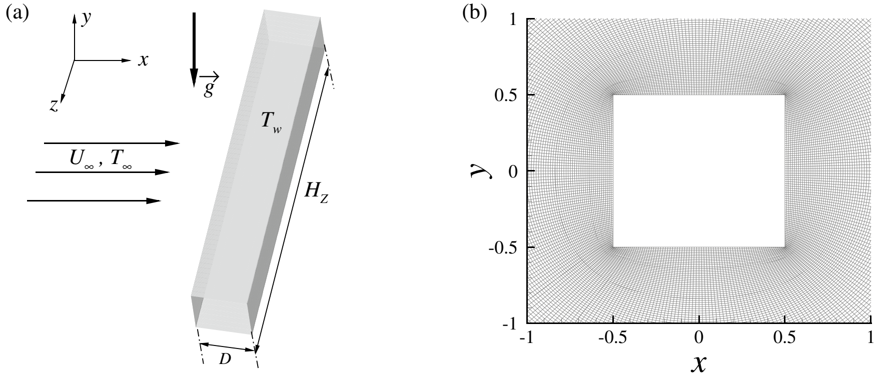

Fig. 1 (**a**) Horizontal flow past a square cylinder, and (**b**) Close view of two-dimensional mesh in $\xi - \eta$ plane

modes having definite spanwise wavelength can be captured by restricting the spanwise domain with a periodic boundary condition, over a finite length $H_z = 6D$ (see Fig. 1a). The flow is described by Cartesian coordinates in which the $x-$, $y-$, and $z-$coordinates are in the streamwise, negative gravity, and spanwise directions, respectively. A circular domain of radius $R = 60D$ is used around a square cylinder whose center is at the same position as the cylinder center. An $O-$type body-fitted mesh is generated with 281, 309, and 61 grid points in the ξ, η, and z directions, respectively. The mesh is initially generated in two-dimensional $\xi - \eta$ coordinates and then uniformly replicated in the $z-$direction. Figure 1b shows a two-dimensional magnified grid with a minimum dimensionless grid size of 1.7×10^{-3}. To capture the flow field on this fine mesh, the dimensionless time-step $\Delta t = 5 \times 10^{-5}$ is employed. In current computations, the Reynolds number, Mach number, and Froude number are kept fixed at $Re = 500$, $M = 0.1$, and $Fr = 1.0$, while the heating level varies from $\epsilon = 0$ to $\epsilon = 1$.

2 Numerical Model

2.1 Governing Equations

The three-dimensional governing equations of compressible gas flow in the strong conservative form are given in non-dimensional form:

$$\frac{\partial \boldsymbol{U}}{\partial t} + \frac{\partial \boldsymbol{F}}{\partial x} + \frac{\partial \boldsymbol{G}}{\partial y} + \frac{\partial \boldsymbol{H}}{\partial z} = \boldsymbol{J}, \tag{1}$$

where $\boldsymbol{U}$ is the solution vector, $\boldsymbol{F}$, $\boldsymbol{G}$, and $\boldsymbol{H}$ denote the flux vectors and $\boldsymbol{J}$ is source vector. These vectors are defined as

$$\boldsymbol{U} = [\rho \quad \rho u \quad \rho v \quad \rho w \quad \rho E]', \tag{2}$$

$$\boldsymbol{F} = \begin{bmatrix} \rho u \\ \rho uu + p - \frac{2\mu}{Re}\left\{\frac{\partial u}{\partial x} - \frac{1}{3}(\nabla \cdot \mathbf{V})\right\} \\ \rho uv - \frac{\mu}{Re}\left(\frac{\partial v}{\partial x} + \frac{\partial u}{\partial y}\right) \\ \rho uw - \frac{\mu}{Re}\left(\frac{\partial u}{\partial z} + \frac{\partial w}{\partial x}\right) \\ \rho uE - \frac{\gamma\kappa}{RePr}\frac{\partial T}{\partial x} + \Phi^F \end{bmatrix}, \qquad \boldsymbol{G} = \begin{bmatrix} \rho v \\ \rho vu - \frac{\mu}{Re}\left(\frac{\partial v}{\partial x} + \frac{\partial u}{\partial y}\right) \\ \rho vv + p - \frac{2\mu}{Re}\left\{\frac{\partial v}{\partial y} - \frac{1}{3}(\nabla \cdot \mathbf{V})\right\} \\ \rho vw - \frac{\mu}{Re}\left(\frac{\partial v}{\partial z} + \frac{\partial w}{\partial y}\right) \\ \rho vE - \frac{\gamma\kappa}{RePr}\frac{\partial T}{\partial y} + \Phi^G \end{bmatrix}, \tag{3}$$

$$\boldsymbol{H} = \begin{bmatrix} \rho w \\ \rho wu - \frac{\mu}{Re}\left(\frac{\partial w}{\partial x} + \frac{\partial u}{\partial z}\right) \\ \rho wv - \frac{\mu}{Re}\left(\frac{\partial w}{\partial y} + \frac{\partial v}{\partial z}\right) \\ \rho ww + p - \frac{2\mu}{Re}\left\{\frac{\partial w}{\partial z} - \frac{1}{3}(\nabla \cdot \mathbf{V})\right\} \\ \rho wE - \frac{\gamma\kappa}{RePr}\frac{\partial T}{\partial z} + \Phi^H \end{bmatrix}, \quad \boldsymbol{J} = \begin{bmatrix} 0 \\ 0 \\ (1-\rho)/Fr^2 \\ 0 \\ (\gamma - 1)\left\{\gamma(1-\rho)\left(\frac{M}{Fr}\right)^2 v - (\nabla \cdot \mathbf{V})\right\} \end{bmatrix}. \tag{4}$$

The terms Φ^F, Φ^G, and Φ^H are given as

$$\Phi^F = \gamma(\gamma - 1)M^2\left(pu + \frac{\mu}{Re}D_F\right), \tag{5}$$

$$\Phi^G = \gamma(\gamma - 1)M^2\left(pv + \frac{\mu}{Re}D_G\right), \tag{6}$$

$$\Phi^H = \gamma(\gamma - 1)M^2\left(pw + \frac{\mu}{Re}D_H\right). \tag{7}$$

The quantities D_F, D_G, and D_H in Eqs. 5–7 are given as

$$D_F = \left[\frac{2}{3}u\left(-2\frac{\partial u}{\partial x} + \frac{\partial v}{\partial y} + \frac{\partial w}{\partial z}\right) - v\left(\frac{\partial v}{\partial x} + \frac{\partial u}{\partial y}\right) - w\left(\frac{\partial w}{\partial x} + \frac{\partial u}{\partial z}\right)\right], \tag{8}$$

$$D_G = \left[\frac{2}{3}v\left(\frac{\partial u}{\partial x} - 2\frac{\partial v}{\partial y} + \frac{\partial w}{\partial z}\right) - u\left(\frac{\partial v}{\partial x} + \frac{\partial u}{\partial y}\right) - w\left(\frac{\partial w}{\partial y} + \frac{\partial v}{\partial z}\right)\right], \tag{9}$$

$$D_H = \left[\frac{2}{3}w\left(\frac{\partial u}{\partial x} + \frac{\partial v}{\partial y} - 2\frac{\partial w}{\partial z}\right) - u\left(\frac{\partial w}{\partial x} + \frac{\partial u}{\partial z}\right) - v\left(\frac{\partial w}{\partial y} + \frac{\partial v}{\partial z}\right)\right]. \tag{10}$$

The above governing equations are closed by thermodynamics state relations which are expressed in dimensionless form:

$$\rho = \frac{1+\gamma M^2 p}{T}, \qquad e = \int_1^T C_v(T)dT + e_\infty, \qquad E = e + \frac{\gamma(\gamma-1)}{2}M^2(u^2+v^2+w^2). \tag{11}$$

The symbols T, ρ, p, κ, μ, e and E represent the temperature, density, thermodynamic pressure, thermal conductivity, viscosity, specific internal energy, and total specific energy, respectively. In the above governing equations, the dimensionless fluid velocities u, v, w are the components of $\mathbf{V}$ in x, y, z directions and t denoted as non-dimensional time. In Eq. 11, the value of e_∞ is taken as unity. The values of κ, C_v are determined using the least squares curve-fitting technique [11, 14, 15], while Sutherland's law is used to calculate the molecular viscosity relation.

2.2 Initial and Boundary Conditions

In the present computations, free-stream values that exist at an infinitely large distance from the cylinder are used to initiate the simulation. At the cylinder surface, a uniform elevated temperature is given and no-slip, no-penetration conditions are used for the velocity. Pressure is determined using normal momentum equations, whereas density is obtained by equation of state. In the spanwise direction, periodic boundary conditions are employed. In order to induce transition to three-dimensionality, a spanwise random perturbation with an order of 10^{-7} is added at the initial condition of the density in the cylinder wake.

At the artificial boundary, the characteristic numerical boundary conditions of the Euler equations based on wave speed along the local normal direction have been applied [16]. At the inflow, where the waves enter the flow region, the characteristic variables are fixed and equal to the free-stream conditions, whereas, at outflow, these attribute variables are extrapolated from the internal values of the domain. For the pressure value at the outflow, the characteristic boundary condition reported in Bayliss and Turkel [17] is employed, which is given as

$$\frac{\partial p}{\partial t} - \left(\frac{1}{M}\right)\frac{\partial V_N}{\partial t} = 0, \tag{12}$$

where V_N is the normal velocity component. The value of density is obtained using the equation of state at the inflow and outflow portion of the domain.

3 Numerical Results

3.1 Validation Study

An in-house compressible solver is validated by comparing the obtained numerical values of the time-averaged drag coefficient and the Strouhal number. The drag coefficient (C_D), the lift coefficient (C_L), and the Strouhal number (St) are defined as

$$C_D = \frac{2F_D}{\rho_\infty {U_\infty}^2 D H_z}, \qquad C_L = \frac{2F_L}{\rho_\infty {U_\infty}^2 D H_z}, \qquad St = \frac{fD}{U_\infty}, \tag{13}$$

where f represents the vortex shedding frequency and F_D, F_L are the integrated forces (drag and lift) on the cylinder. At $Re = 200 - 300$ and $\epsilon = 0$, the obtained numerical values of St and $\overline{C_D}$ are compared with the reported values obtained via DNS, experimental, and Floquet methods as listed in Tables 1 and 2. The St values in the present study are calculated by the dominant frequency obtained using FFT algorithm of time history of lift coefficient (C_L). Table 1 shows that the St values of the present study are very close to the values of the DNS study reported by Jiang et al. [5], with a maximum deviation of 4%. Similarly, the $\overline{C_D}$ values are well validated by the values reported by Jiang and Cheng [18] with deviations less than 3%, as listed in Table 2.

Table 1 Comparison of Strouhal number (St) for various Re at $\epsilon = 0$

Re	Present study DNS	Jiang et al. [5] DNS	Mahir [19] DNS	Okajima [20] Exp.	Luo et al. [1] Exp.
200	0.1445	0.1490	0.154	0.1395	0.159
220	0.1457	0.1504	0.151	–	0.159
230	0.1466	0.1510	0.154	–	0.161
250	0.1452	–	0.152	0.1421	0.159
300	0.1391	0.1453	–	0.1399	–

Table 2 Comparison of time-averaged drag coefficients ($\overline{C_D}$) for various Re at $\epsilon = 0$

Re	Present study DNS	Jiang and Cheng [18] DNS	Sohankar et al. [3] DNS	Mahir [19] DNS	Robichaux et al. [2] Floquet
200	1.405	1.393	1.459	1.518	1.642
220	1.432	1.41	–	1.554	1.671
250	1.451	–	1.491	1.567	1.73
300	1.479	1.438	1.561	–	1.873

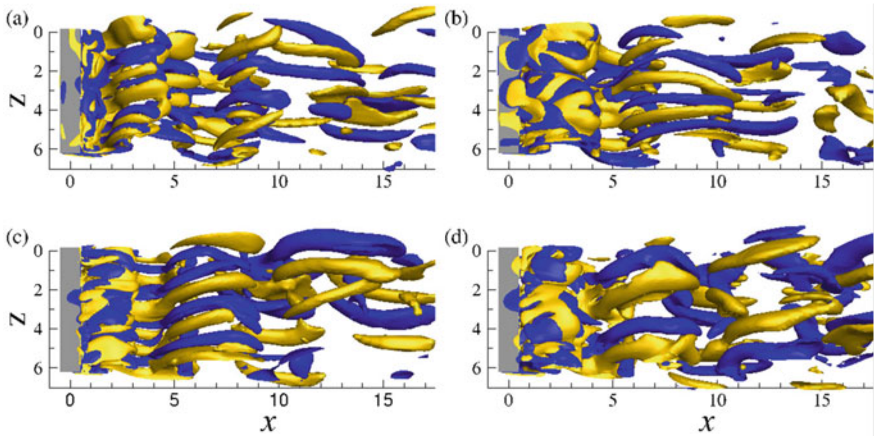

Fig. 2 Iso-surfaces of $\omega_x = \pm 0.5$ in the square cylinder wake at $Re = 500$ and $t = 900$ for (**a**) $\epsilon = 0.0$, (**b**) $\epsilon = 0.2$, (**c**) $\epsilon = 0.6$, and (**d**) $\epsilon = 1.0$. Yellow and blue represent positive and negative values, respectively

3.2 Vortical Structure

The three-dimensional flow in a bluff body wake depends on several factors such as bluff body shape, incoming flow, and buoyancy effect. The strong buoyancy causes the flow field to become asymmetric and significantly changes the shape of the vortical structure in the cylinder wake. Figure 2 shows the vortical structures of streamwise vorticity (ω_x) in a square cylinder wake with different heating at $Re =$ 500. The disordered vortical structure of the mode B transition is observed in square cylinder wake at $\epsilon = 0$ as shown in Fig. 2a. On increasing the heating level from $\epsilon = 0$ to $\epsilon = 0.6$, the vortical structures with $\lambda_z = 1.2D - 1.5D$ (depending on the vortex pair in the cylinder wake) do not change significantly (see Fig. 2a–c). Further increasing the heating value to $\epsilon = 1.0$, the strong effect of buoyancy transformed the disordered mode B structure into the mode C structure with wavelength $\lambda_z \sim 3D$ (see Fig. 2d).

3.3 Time Histories of Force Coefficients

Figure 3 shows the time history of C_D and C_L for $\epsilon = 0.0$ and $\epsilon = 1.0$ at $Re = 500$. Based on this plot, the amplitude of both the drag and the force coefficient becomes smaller with increase in the heating of the cylinder. The mean value of C_D decreases slightly on large-scale heating ($\epsilon = 1.0$), while the average value of C_L changes significantly with heating and gives negative values (see in Fig. 3b). This negative value of C_L at strong buoyant force is observed due to unbalanced pressure and shear forces around the cylinder developed by the asymmetric flow field.

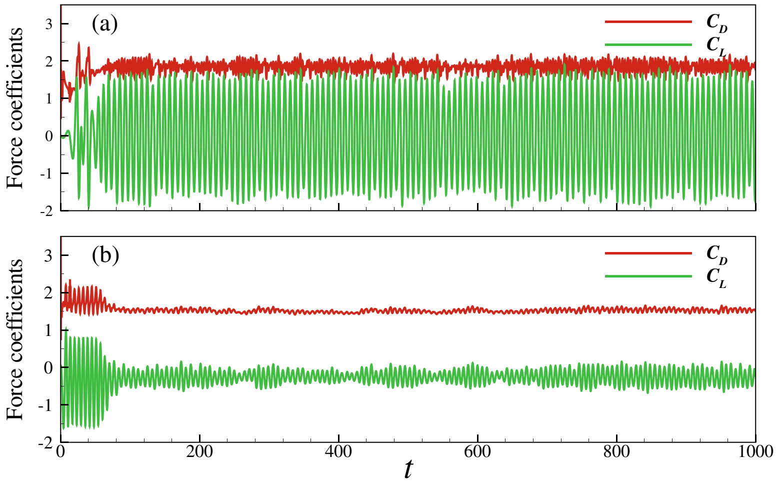

Fig. 3 Time histories of force coefficients (C_D and C_L) at $Re = 500$ for (**a**) $\epsilon = 0.0$ and (**b**) $\epsilon = 1.0$

3.4 *Frequency Spectra of Lift Coefficient*

Figure 4 shows the amplitude of C_L, with the St value at $Re = 500$ for $\epsilon = 0.0$ and $\epsilon = 1.0$. The vortex shedding frequency spectra are obtained from the Fast Fourier Transform (FFT) algorithm using the time history of the C_L values. At $\epsilon = 1.0$, the amplitude of C_L is about 10 times less than that of C_L amplitude of the unheated case (see Fig. 4). Additionally, the dominant peak frequency of the vortex shedding (i.e., St value) slightly increases upon heating of the cylinder surface ($\epsilon = 1.0$).

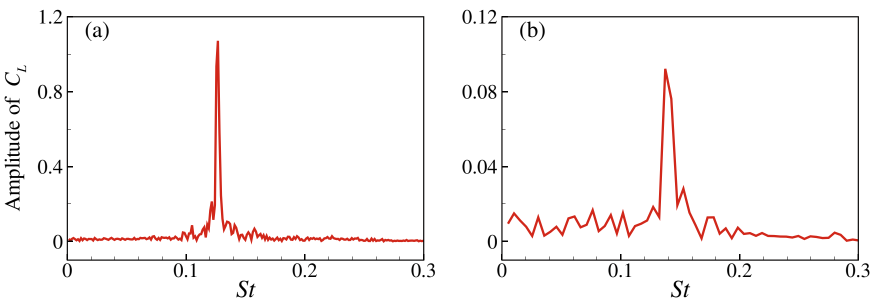

Fig. 4 At $Re = 500$, frequency spectra of lift coefficient (C_L) with heating (**a**) $\epsilon = 0.0$ and (**b**) $\epsilon = 1.0$

4 Conclusions

This paper presents a DNS study of the three-dimensional flow around a heated square cylinder subjected to a uniform free stream ($Pr = 0.7$) at right angle to gravity. At $Re = 500$, the disordered mode B vortical structure with $\lambda_z = 1.2D - 1.5D$ is observed in the isothermal wake behind the unheated square cylinder ($\epsilon = 0.0$). At $\epsilon = 0 - 0.6$, the vortical structure does not change significantly and the value of λ_z remains the same. At large-scale heating ($\epsilon = 1.0$), a significant changes is observed in the shape of the vortical structure with wavelength $\lambda_z \sim 3D$. The flow field around the heated cylinder becomes asymmetric due to the non-parallelism between the free-stream crossflow and buoyancy. The asymmetric flow field creates unbalanced pressure and shear forces that lead to the generation of negative lift. The amplitude of C_L becomes smaller as the buoyant force increases. Additionally, when the heating level is increased from $\epsilon = 0$ to $\epsilon = 1$, there is a very slight increase in the St value of the vortex shedding.

Acknowledgements The authors would like to acknowledge the computational support provided by the High-Performance Computing Facility at the Indian Institute of Technology, Delhi, India.

References

1. Luo S, Chew Y, Ng Y (2003) Characteristics of square cylinder wake transition flows. Phys Fluids 15:2549–2559
2. Robichaux J, Balachandar S, Vanka S (1999) Three-dimensional Floquet instability of the wake of square cylinder. Phys Fluids 11:560–578
3. Sohankar A, Norberg C, Davidson L (1999) Simulation of three-dimensional flow around a square cylinder at moderate Reynolds numbers. Phys Fluids 11:288–306
4. Agbaglah G, Mavriplis C (2017) Computational analysis of physical mechanisms at the onset of three-dimensionality in the wake of a square cylinder. J Fluid Mech 833:631–647
5. Jiang H, Cheng L, An H (2018) Three-dimensional wake transition of a square cylinder. J Fluid Mech 842:102–127
6. Sheard GJ, Fitzgerald MJ, Ryan K (2009) Cylinders with square cross-section: wake instabilities with incidence angle variation. J Fluid Mech 630:43–69
7. Roshko A (1954) On the development of turbulent wakes from vortex streets
8. Kieft RN, Rindt C, Van Steenhoven A, Van Heijst G (2003) On the wake structure behind a heated horizontal cylinder in cross-flow. J Fluid Mech 486:189–211
9. Ren M, Rindt CC, Van Steenhoven AA (2006) Three-dimensional transition of a water flow around a heated cylinder at $re = 85$ and $ri = 1.0$. J Fluid Mech 566:195–224
10. Mahir N, Altaç Z (2019) Numerical investigation of flow and combined natural-forced convection from an isothermal square cylinder in cross flow. Int J Heat Fluid Flow 75:103–121
11. Arif MR, Hasan N (2019) Vortex shedding suppression in mixed convective flow past a square cylinder subjected to large-scale heating using a non-Boussinesq model. Phys Fluids 31:023602
12. Arif MR, Hasan N (2020) Effect of thermal buoyancy on vortex-shedding and aerodynamic characteristics for fluid flow past an inclined square cylinder. Int J Heat Technol 38:463–471
13. Arif MR, Hasan N (2021) Effect of free-stream inclination and buoyancy on flow past a square cylinder in large-scale heating regime. Phys Fluids 33:073601

14. Ghoshdastidar PS (2012) Heat transfer. Oxford University Press. https://books.google.co.in/books?id=DxeKpwAACAAJ
15. Hasan N, Saeed A (2017) Effects of heating and free-stream orientation in two-dimensional forced convective flow of air past a square cylinder. Int J Therm Sci 112:1–30
16. Hirsch C (2007) Numerical computation of internal and external flows: the fundamentals of computational fluid dynamics. Elsevier
17. Bayliss A, Turkel E (1982) Far field boundary conditions for compressible flows. J Comput Phys 48:182–199
18. Jiang H, Cheng L (2018) Hydrodynamic characteristics of flow past a square cylinder at moderate Reynolds numbers. Phys Fluids 30:104107
19. Mahir N (2017) Three dimensional heat transfer from a square cylinder at low Reynolds numbers. Int J Therm Sci 119:37–50
20. Okajima A (1982) Strouhal numbers of rectangular cylinders. J Fluid Mech 123:379–398